JACS
JOURNAL OF THE AMERICAN CHEMICAL SOCIETY
Article
pubs.acs.org/JACS

Excited-State Dynamics of Oxyluciferin in Firefly Luciferase

Joris J. Snellenburg,[†,¶] Sergey P. Laptenok,[‡,¶,#] Richard J. DeSa,[§] Panče Naumov,[*,⊥] and Kyril M. Solntsev[*,∥,§]

[†]Faculty of Sciences, Department of Physics and Astronomy, VU University Amsterdam, 1081 HV Amsterdam, The Netherlands
[‡]School of Chemistry, University of East Anglia, Norwich Research Park, Norwich NR4 7TJ, United Kingdom
[§]Olis, Inc., 130 Conway Drive, Bogart, Georgia 30622, United States
[⊥]New York University Abu Dhabi, P.O. Box 129188, Abu Dhabi, United Arab Emirates
[∥]School of Chemistry and Biochemistry, Georgia Institute of Technology, 901 Atlantic Drive, Atlanta, Georgia 30332-0400, United States

Supporting Information

ABSTRACT: The color variations of light emitted by some natural and mutant luciferases are normally attributed to collective factors referred to as microenvironment effects; however, the exact nature of these interactions between the emitting molecule (oxyluciferin) and the active site remains elusive. Although model studies of noncomplexed oxyluciferin and its variants have greatly advanced the understanding of its photochemistry, extrapolation of the conclusions to the real system requires assumptions about the polarity and proticity of the active site. To decipher the intricate excited-state dynamics, global and target analysis is performed here for the first time on the steady-state and time-resolved spectra of firefly oxyluciferin complexed with luciferase from the Japanese firefly (*Luciola cruciata*). The experimental steady-state and time-resolved luminescence spectra of the oxyluciferin/luciferase complex in solution are compared with the broadband time-resolved firefly bioluminescence recorded in vivo. The results demonstrate that de-excitation of the luminophore results in a complex cascade of photoinduced proton transfer processes and can be interpreted by the pH dependence of the emitted light. It is confirmed that proton transfer is the central event in the spectrochemistry of this system for which any assignment of the pH-dependent emission to a single chemical species would be an oversimplification.

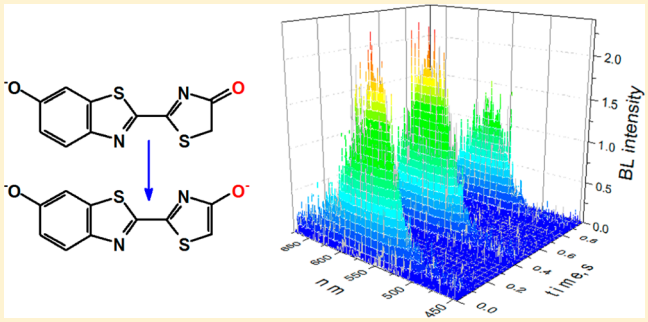

INTRODUCTION

The rare combination of highest photoyield among the natural bioluminescence (BL) reactions with exogenic precursors,[1,2] easy synthetic access to the substrate (luciferin), and availability of the enzyme (luciferase, Luc) turns firefly BL into the most favorable BL system with an exogenous substrate for in vivo imaging as well as for other bioanalytical applications.[3−11] However, the studies into the possible application have not been paralleled with advancement in the understanding of the related reaction mechanisms. Indeed, despite the burgeoning model studies on the underlying photochemistry, even very fundamental mechanistic aspects such as the true chemical identity of the emitting species, oxyluciferin ($OxyLH_2$), as well as its ultrafast dynamics and de-excitation pathways after it has been generated in the active site of Luc remain unknown. A number of recent spectroscopic studies of the noncomplexed luminophore and its derivatives in model solutions have been directed to shed light on its intricate photochemistry.[12−21] The possibility of having complex mixtures of up to six (in neutral or basic pH) interconvertible chemical forms of $OxyLH_2$ in such solutions (Figure 1), the dependence of the three chemical equilibria on the solvent composition and pH, and the proclivity of the emitter for dimerization in basic conditions[22] pose major hurdles for modeling the $OxyLH_2$ spectrochemistry.[18] Although the results from model solution studies are useful for their exactness and technical feasibility, implicit or direct extrapolation to the dynamics of the emitter in Luc under real physiological conditions is always subject to assumptions related to the nature of the interactions with the active site. In the absence of reliable experimental benchmarks, the computational studies have anteceded the experimental research, and thorough theoretical models to describe the generation of the emitter and its interaction with the active pocket of Luc have been developed.[23−31]

According to the reaction mechanism of the firefly BL that was originally advanced,[32] $OxyLH_2$ is generated via thermal decomposition of a chemiexcited unstable intermediate in its (ionic) *keto* form, although there are also arguments that point to emission from its enol tautomer and/or the neutral

Received: May 29, 2016
Published: November 23, 2016

DOI: 10.1021/jacs.6b05078
J. Am. Chem. Soc. 2016, 138, 16252−16258

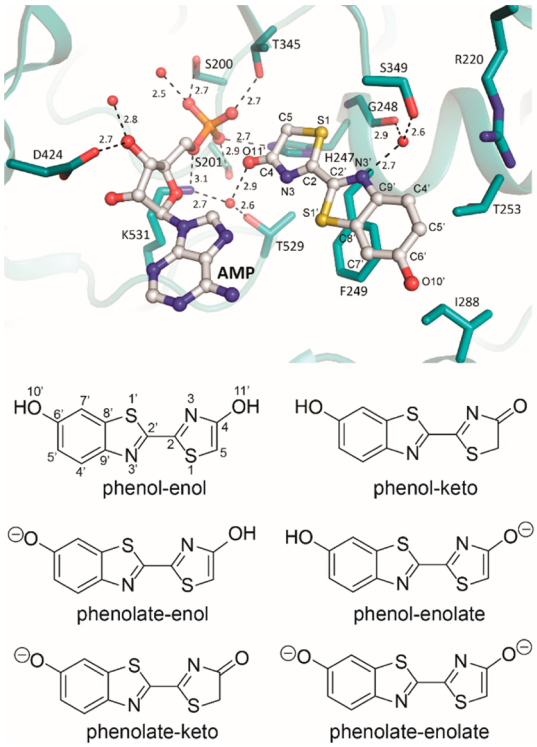

Figure 1. Firefly oxyluciferin ($OxyLH_2$), shown with the atom labeling scheme, in the interior of luciferase from the Japanese firefly (*L. cruciata*) (PDB code: 2D1R) and possible chemical forms of $OxyLH_2$ in neutral and basic solutions (additional protonated species are possible in acidic solution). The chemical form of the ground-state oxyluciferin was originally assigned as the keto−phenol tautomer;[37] however, there is crystallographic evidence that the actual tautomer in the ground state is the enol−phenol form.[12]

form.[12,15,16,33] The "keto hypothesis"[34] clearly contrasts the tautomeric form, which was observed in a single crystal and as the major component in polar solutions, where the molecules are stabilized and exist as neutral hydrogen-bonded dimers of the enol tautomer.[12,35,36] Furthermore, inspection of the bond distances of the emitter in the crystal structure of luciferase from *Luciola cruciata*[37] shows that in the ground state $OxyLH_2$ exists as the neutral *enol* form.[12] Although simulations of the molecular dynamics indicate that any significant reorganization of the microenvironment would occur at ultrafast time scales,[31] stabilization of the enol form by a nearby leaving adenosine monophosphate (AMP, Figure 1) could account for the enol form being the resting (ground) state of the emitter within the enzyme.[12]

It has been suggested[26] that the possibility of π-stacking is also involved in stability of the enol tautomer. While this is definitely a possibility in solution, the stacking is not possible in the enzyme, where only one molecule of the emitter can be incorporated in the active site. Surprisingly, the preliminary results on the picosecond-to-nanosecond dynamics of $OxyLH_2$ and its analogues[16] in model solutions have revealed stronger photoacidity of the enol group relative to the phenol group—an indication of excited-state proton transfer (ESPT) pathway(s) that could be initiated by excited-state keto−enol tautomerization. Further theoretical study provided an explanation for this phenomenon.[33] Moreover, the action spectra of a complex of the emitter with a water molecule in vacuo have concluded[17] that reversible interaction with a single water molecule could have a profound effect on the absorption/emission energy and have advanced water as a possible moderator of the emission color. In solution, multivariate curve resolution/alternating least squares analysis of the pH-dependent spectra has provided for the first time the absorption[18] and emission[36] spectra of the individual chemical forms of $OxyLH_2$ free from contributions from the other forms, their pH-dependent profiles and distributions, and accurate values for the three equilibrium constants (two deprotonation constants and keto−enol tautomerism).

In model aqueous solutions, the ground-state $OxyLH_2$ can exist as a chemical equilibrium between some of the six species that absorb in a relatively narrow range (367−486 nm) at pH 6−11 (Figure 1).[12,18] The close values of the two pK_a (9.10 ± 0.12 and 7.40 ± 0.15 for the phenol/phenolate and enol/enolate, respectively) afford approximately 2:1:1 for the ratio of populations of the phenol−enol/phenol−keto/phenol−enolate forms at pH 7.[18,36] It has been established that in aqueous solution the latter distribution of the absorbing species results in their simultaneous excitation and photochemical transformations.

To obtain direct insight into the excited-state dynamics of this system, we have resorted to time-resolved fluorescence. Herein, the results of a thorough sub-nanosecond spectroscopic study of $OxyLH_2$ in complex with Luc ($OxyLH_2$@Luc) from the Japanese firefly (*L. cruciata*) are presented. This approach is justified by the identity of the fluorescent and bioluminescent states, which was established by computational methods recently.[30] The resulting photoinduced dynamics of $OxyLH_2$@Luc was analyzed by global and target analysis with the intention to decipher all photochemical pathways that are possible in the luciferase active pocket, at least in principle. We note that due to the complex chemical nature of the emitter, normally multiple chemical forms of $OxyLH_2$ are simultaneously excited; under such conditions, the present results reveal the *possible* rather than *most probable* pathways. Alternative approaches to monitor the ultrafast dynamics of the actual chemiluminescence reaction are not feasible because of the slow triggering of the chemical reaction by diffusion-controlled processes (diffusion of ATP or Mg^{2+}) and the slow empirical kinetics of the subsequent light emission (seconds). The chemical forms and the excited-state pathways of the emitter in the active pocket of the enzyme at three pH values are reported for the first time. The spectral fingerprint is modeled as a result of complex multicomponent ESPT. The results set the benchmark for further computational studies into the microenvironment effects on the de-excitation pathways and various colors emitted by the natural and mutant firefly luciferases.

MATERIALS AND METHODS

Preparation of the Samples. $OxyLH_2$ was synthesized as described elsewhere.[12] Recombinant luciferase from *L. cruciata* (Japanese firefly) was purchased from Wako (Japan). The complexes of $OxyLH_2$ with Luc in aqueous buffer solutions with various pH were prepared as follows (Table S1, Supporting Information): 20 mL of aqueous suspension containing ~2 mg of $OxyLH_2$ was thoroughly shaken for 15−20 min and diluted with 20 mL of freshly prepared phosphate buffer (200 mM) containing AMP (1.25 mM) and $MgSO_4$ (0.4 mM). The mixture was filtered, added to fresh solution of the enzyme (3 mg) in 15 mL of phosphate buffer (100 mM), and incubated 5−10 min at 37 °C. This procedure was performed very rapidly for the basic solution to avoid decomposition. The pH of the resulting solution was measured. For the in vivo experiments, a

DOI: 10.1021/jacs.6b05078
J. Am. Chem. Soc. 2016, 138, 16252−16258

flashing living firefly was collected by one of us (R.J.D.) on a farm near Jefferson, Georgia, USA, in June 2015. The bug was placed freely into standard 1 cm^2 cuvette, and the emission was stimulated by gentle tapping with a cotton swab.

Time-Resolved Spectroscopy and Global Analysis. The time-resolved fluorescence was measured on the time-correlated single-photon counting Edinburg Instrument apparatus described in a previous publication.[16] The millisecond broadband BL from a living firefly was taken using the OLIS RSM1000 spectrometer. As in the previous work,[16] the global and target analysis[41] of the time-resolved fluorescence data was performed using the publicly available package Glotaran 1.5.1.[46,47]

The data were analyzed by means of global analysis (at every measured wavelength, the data were fitted by a sum of exponential decays convoluted with the instrument response function, IRF). The amplitudes that are estimated for each decay curve represent the estimated spectra, with a lifetime given by the inverse of the rate constant that describes the exponential decay. The simplest form of global analysis uses a model of a number of parallel decaying components where the corresponding estimated amplitudes at each wavelength are termed decay-associated spectra (DAS). A positive amplitude means a fluorescence decay, whereas a negative amplitude means a rise of fluorescence with that lifetime. A DAS which is positive in one region of the measured wavelength range and negative in another can be indicative of excited-state population transfer with the lifetimes associated with that component. When no spectral constraints are used, the combination of lifetimes and corresponding DAS represent a pure mathematical decomposition of the data, provided that the residual is sufficiently structureless. It is important to note that the DAS therefore do not necessarily represent the spectra of pure physical (chemical) species but rather a mixture of states with similar lifetimes.

A more advanced form of the global analysis uses a kinetic model of interconnected components where each microscopic rate constant represents the transfer of population of one (excited-state) species into another or the decay to the ground state. Typically, spectral constraints are then required to estimate all components. The spectra resulting from such an analysis are termed "species associated spectra" (SAS) and are thought to represent the pure physical or chemical (excited-state) species. The appropriateness of this assumption depends strongly on the correctness of the model and whether or not the different species can be either kinetically or spectrally distinguished given the finite time resolution and spectral resolution of the experiment. The millisecond broadband BL was also analyzed using Glotaran. First the data set was split into one data set for each of the three observed luminescence bursts. Next, a single model for all three data sets was defined consisting of a Gaussian IRF and a single decay rate. Then only the position parameter was unlinked between data sets to allow for a different starting position. All parameters were then optimized, and the data were fitted up to the noise level.

RESULTS AND DISCUSSION

Steady-State Spectra. Buffered solutions of the complex of pure synthetic $OxyLH_2$ with Luc from *L. cruciata* were prepared at pH 6.8, 7.8 and 8.3, and the excitation−emission spectra were recorded. The excitation−emission spectra, together with those for $OxyLH_2$ in aqueous buffer at pH 7.0, are depicted in Figure S1, Supporting Information. From these data, the normalized absorption spectra (Figure 2a) and the emission maximum as a function of excitation wavelength (Figure 2b) were extracted.

Similar to aqueous solutions,[18] the absorption maxima of $OxyLH_2$@Luc exhibit a bathochromic shift with increasing pH in response to the gradual deprotonation of $OxyLH_2$. However, the absorption band of $OxyLH_2$@Luc at pH 6.8 was considerably broadened relative to that of $OxyLH_2$ in water at comparable pH (Figure 2a). This broadening is indicative of contribution from a broader spectrum of a ground-state species.

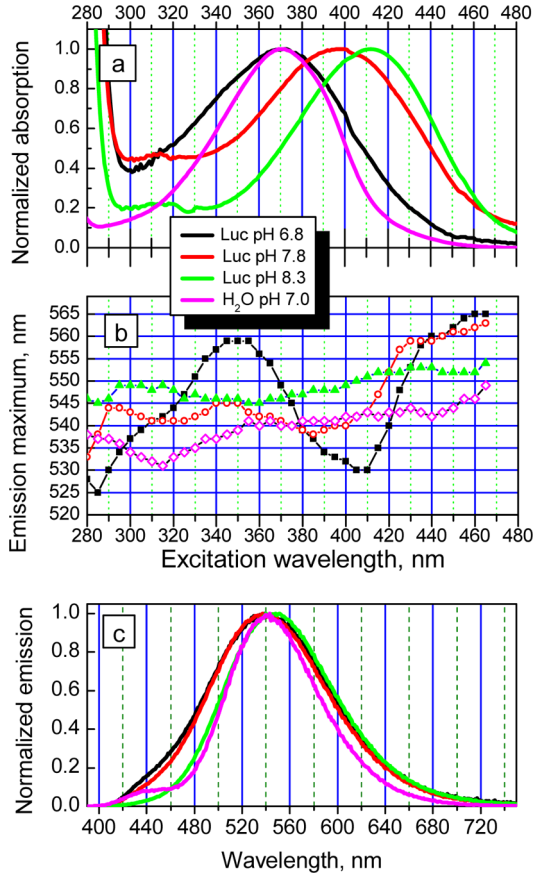

Figure 2. (a) Absorption spectra of $OxyLH_2$ in aqueous buffered solutions of Luc at various pH. The absorption spectrum in water at pH 7.0 is shown for comparison. (b) Dependence of the major emission maxima at each pH on the excitation wavelength. (c) Emission spectra of $OxyLH_2$ in aqueous buffered solutions of Luc at various pH after 380 nm excitation. The emission spectrum in water at pH 7.0 is shown for comparison. The color coding is the same for all graphs.

The fluorescence spectra of the systems described above are presented in Figure 2c. In the earlier reports,[38,39] the fluorescence spectrum of $OxyLH_2$ in water at neutral pH was treated as a two-band emission. The weak shoulder at 450 nm was assigned to the neutral species and the dominating emission at 550 nm to the conjugate base formed via ESPT. The same behavior was observed here for $OxyLH_2$@Luc at all pH values. As pH increased, the relative contribution of the 450 nm shoulder decreased due to ground-state deprotonation that leads to the disappearance of neutral species from the ground state and, consequently, from the excited state. Also, the recent data on tautomeric equilibrium of $OxyLH_2$ in aqueous solutions[18] demonstrated contribution from more than one species in the 350−400 nm region where $OxyLH_2$ is usually excited to record steady-state and time-resolved emission.

Time-Resolved Emission. To investigate the nature of the difference in the emission behavior between $OxyLH_2$ and $OxyLH_2$@Luc at neutral pH, time-resolved emission data on the latter were recorded using a time-correlated single-photon counting setup under two different excitation wavelengths, 372 and 467 nm (for details, see Figure S2, Supporting Information, and the Materials and Methods section), and three pH (for clarity, hereafter spectra recorded at pH 6.8, 7.8, and 8.3 are labeled e1, e2, and e3, respectively). Representative fluores-

DOI: 10.1021/jacs.6b05078
J. Am. Chem. Soc. 2016, 138, 16252−16258

cence decay traces for 372 nm excitation are shown in Figure S3. The complete time-resolved emission maps in the studied conditions, including the raw data, are presented as Figure S2, Supporting Information. Figure 3 shows very different kinetics

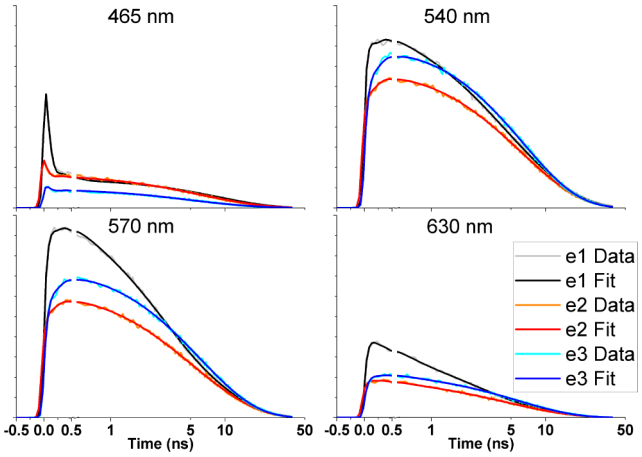

Figure 3. Representative decay traces at 465, 540, 570, and 630 nm. For e1, e2, and e3, the respective raw data are shown in gray, orange, and cyan, and the fitted traces are overlaid in black, red, and blue. The *y* axis for all traces is normalized to 10^4 counts.

at various selected wavelengths; under such circumstances, analysis at a single emission wavelength is not a viable approach, and global analysis is necessary to disentangle the individual spectra and the corresponding kinetics contributing to the signal.

Global Analysis. For each excitation wavelength, the time-resolved emission data from the three pH values (e1, e2, e3) were simultaneously analyzed by means of linked global analysis. Rather than analyzing each data set individually, which would require a total of 14 rate constants and corresponding spectra, the assumption was made that all data sets could be described by the same sets of spectral and kinetic parameters, albeit in varying amount, to reflect the pH-dependent changes in ground-state populations. Overall, only seven kinetic parameters and corresponding spectra were found to be necessary for a satisfactory fit of the data. The IRF was assumed to be invariable across the three data sets at a given excitation wavelength and was modeled after a measurement of pure scatter. The estimated global lifetimes (the reciprocal of the estimated rate constants) are summarized in Table 1. The

Table 1. Lifetimes (ns) Estimated from the Global Analysis Emission Lifetimes of Firefly Oxyluciferin in Luciferase of *L. cruciata* ($OxyLH_2$@Luc)

ex/nm	t_1	t_2	t_3	t_4	t_5	t_6	t_7
372	0.04	0.15	0.35	2.1	5.0	7.2	11
467	scatter	0.12	0.41	2.2	6.0	7.4	6.0

normalized DAS associated with these lifetimes are shown in Figure 4, and the corresponding input (reflecting the relative scaling) for each component is given per data set in Table S1, Supporting Information.

The fastest lifetime (black DAS) that can be resolved by careful deconvolution with the fitted IRF is ≈50 ps. It can only be reliably estimated in the case of the 372 excitation. It features primarily fluorescence decay with a maximum around

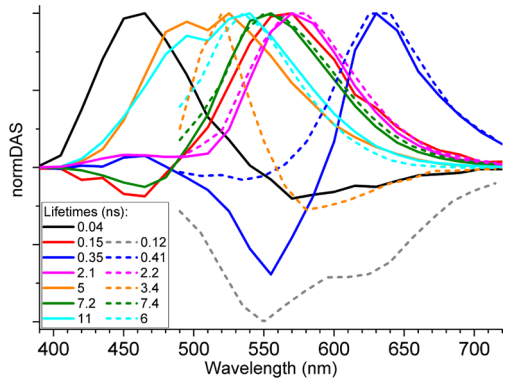

Figure 4. Estimated decay-associated spectra with corresponding lifetimes t_1 (black), t_2 (red), t_3 (blue), t_4 (green), and t_5 (magenta) listed in Table 1. Excitation at (a) 372 nm (solid lines) and (b) 467 nm (dashed lines).

460 nm. Concomitant with this decay, a smaller rise of emission above 550 nm was observed. This component has, by far, the largest amplitude in the e1 sample, as can be clearly seen from the 465 nm trace in Figure 3, and decreases with increasing pH; see also Table S1. The second component in the 372 nm excitation data (solid red DAS) has a lifetime of about 160 ps and represents a fast decay with a maximum around 560 nm. Again, it is most clearly observed in the e1 data set. In the 467 nm excitation, the first lifetime that can be estimated is about 120 ps, but it is virtually only present in the e3 data set and could also be modeled using a stretched IRF. Provided that it is real and not related to a different IRF for this data set,[40] the bimodal character would suggest a relatively slow rise of fluorescence in two bands peaking around 550 and 630 nm upon photoexcitation at 467 nm and more with higher pH. The third component (blue DAS) has a lifetime of around 0.4 ns and a clear peak around 630 nm. In the 372 nm excitation data, there is a clear rise of fluorescence around 550 nm on the same time scale, which is seemingly absent in the 467 nm excitation. The fourth component (magenta DAS) has a lifetime of around 2 ns. It is spectrally virtually identical in both excitation conditions and characterized by a maximum around 570 nm. Its amplitude decreases consistently with increasing pH. It has a notably high amplitude around 460 nm where the red, blue, and green DAS also have significant amplitudes alternating between positive and negative. This multiexponential character with alternating amplitudes is indicative of a non-exponential recombination process resulting in 460 nm emission at multiple time scales. The sixth component (green DAS) represents another well-defined state with a lifetime around 7 ns and a spectrum peaking around 550 nm.

The fifth (orange DAS) and seventh (cyan DAS) components represent long-lived emission peaking between 520 and 540 nm. Although the peak emission from these DAS align well, their spectral shapes are different. In the 372 excitation data both DAS seem to have some additional band around 495 nm (which likely is not excited at 467 nm) and are relatively longer lived (5 and 11 ns, respectively). With excitation at 467 nm, the lifetimes are shorter (3.4 and 6 ns) and the spectra appear narrower. Furthermore, the 3.4 ns DAS also features some energy transfer process to a redder species on this time scale. Overall, the kinetics between the two excitation wavelengths is largely consistent and the spectral shapes are similar; however, the 372 nm excitation data clearly

DOI: 10.1021/jacs.6b05078
J. Am. Chem. Soc. 2016, 138, 16252−16258

allow more spectra to be resolved. Consequently, only these data were used in the target analysis.[31]

Target Analysis. The goal of a target model is to disentangle the recorded fluorescence possibly originating from six different chemical species as described in Figure 1. Each species potentially has nonzero absorption at the combination of excitation wavelength and pH and is potentially associated with its own set of photoinduced processes. The target model that gave the best fit to the data is depicted in Scheme 1, and the estimated normalized SAS are shown in Figure 5.

Scheme 1. Target Model for Oxyluciferin in the Active Site of Firefly Luciferase[a]

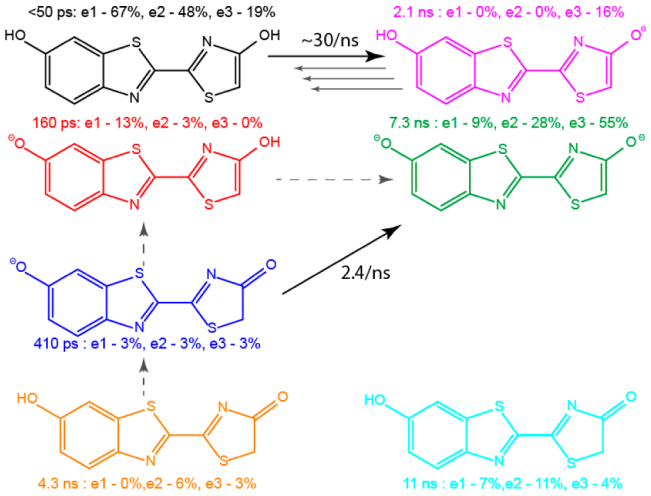

[a]Chemical forms: phenol−enol (black), phenol−enolate (magenta), phenolate−enol (red), phenolate−keto (blue), phenolate−enolate (green), and two states of phenol−keto (orange and cyan). Lifetimes and relative ground-state absorption are as indicated. Solid lines represent directly observed transfer of excited-state population. The possible transfer is indicated by dashed lines, and multiexponential geminate recombination is shown by three thin solid arrows.

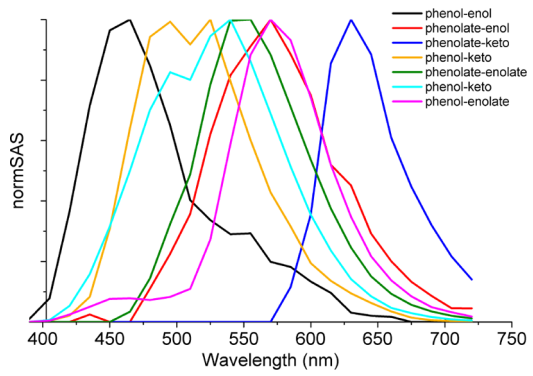

Figure 5. Normalized species-associated spectra (normSAS) resulting from target analysis of the spectra obtained with excitation at 372 nm.

The key assumption we have made here is that the spectral shapes can be linked between data sets, which implies the spectral shapes do not change significantly for the different pH values. In addition, the rate of energy transfer and fluorescence decay is assumed to be pH-independent. This might not necessarily be the case, but on the basis of the quality of the fit, these assumptions work quite well.

Based on earlier work, we assign the bluest emitter to phenol−enol (black SAS) and the reddest emitter to phenolate−keto (blue SAS).[16,36] The fastest process observed in global analysis is described in the target model by (partial) ESPT from phenol−enol to the magenta species, which is assigned to the phenol−enolate form (magenta SAS). Without information or a prior assumption on the relative oscillator strength of the two species, the loss due to ESPT and to direct decay to the ground state could not be quantified. Geminate recombination in relation to this ESPT process[16] is also observed at multiple time scales, but it was not explicitly included in the target model, resulting in a shoulder in the emission of phenol−enolate around 460 nm. Another photoinduced process already suggested in previous work[16] is directly observed in the present experiments—the conversion from phenolate−keto to phenolate−enolate. This result allows us to assign the green SAS to the phenolate−enolate.

With four out of six chemical identities resolved, three species remained unassigned. As suggested by Ghose et al.,[36] the phenol−keto species shows emission around 520 nm and is shifted to the blue relative to the phenolate−enolate form. In this region, our target analysis reveals two distinct contributions with a broad emission centered around 510−520 nm having significantly different lifetimes. We assign both SAS to different conformation in the protein binding pocket of the phenol−keto form (the dip in both spectra around 510 nm could be an artifact of the measurement or indication to bimodal nature of these states). The 467 nm excitation data suggest the latter alternative is more likely because there the 495 nm band appears to be completely missing, possibly because this band is not excited at this wavelength. The 372 nm excitation data do not provide the evidence for direct ESPT from the phenol−keto, but the 467 nm excitation data seem to suggest that there could be some for the shortest lived phenol−keto to phenolate−keto species; accordingly, it was included as a possible energy transfer step in the target model. The last species that remains unassigned is the phenolate−enol form. By exclusion, we assign it to the remaining unassigned red SAS, which is also in agreement with the report of Ghose et al.[36] In our target model, the phenolate−enol decays directly to the ground state; however, the alternative—(partial) ESPT from phenol−enolate to phenolate−enolate—cannot be excluded due to the limited time resolution of the experiment. Moreover, an alternative pathway of the tautomerization of the phenolate−keto species via phenolate−enol cannot be excluded (indicated by dashed arrows in Scheme 1).

The target model allows decomposition of the steady-state emission spectra into individual contributions (Table 2). The primary emitters found are the phenolate−enolate, phenol−enolate, and phenol−keto forms. With increasing pH, phenolate−enolate becomes, by far, the dominant contributor to the fluorescence emission.

Table 2. Total Contributions to the Steady-State Spectrum of $OxyLH_2$@Luc

pH	phenol−keto	phenolate−enolate	phenol−enolate	sum
6.8	41.1%	39.6%	16.5%	97.2%
7.8	43.3%	50.1%	5.8%	99.2%
8.3	14.5%	81.3%	3.8%	99.6%

The global/target analysis results obtained in this work conform to the proposed decay scheme for $OxyLH_2$ in water.[35]

DOI: 10.1021/jacs.6b05078
J. Am. Chem. Soc. 2016, 138, 16252−16258

Of course, the relative distribution of the ground-state species and their absolute spectral assignments are heavily influenced by the microenvironment of the luciferase binding site. To arrive at more direct inferences on the real system, we compared the luminescence of the OxyLH2@Luc complex with the BL of a firefly recorded in vivo.

Comparison of the Light Output of OxyLH$_2$@Luc and Luciferase in Vivo. Whole-body BL imaging is rapidly developing.[42,43] However, to our knowledge, a whole-body broadband spectroscopy of fireflies is extremely rare, and the few reported studies of such measurements were performed using anesthetized and immobilized insects.[44,45] In all cases, a narrow (fwhm 80 nm) BL emission peak with the maximum in the 540−550 nm spectral region was detected.

Using an OLIS RSM1000 spectrometer, we were able to record the broadband emission from a live firefly with temporal resolution of 1 ms. The data set (Figure S4, Supporting Information) was analyzed globally and characterized by a single Gaussian IRF (fwhm 0.0372 s) and a single decay rate of 56.4 ± 0.4/s, that is, a lifetime of 18 ms. The principal spectral BL component and its kinetic behavior are shown in Figure 6.

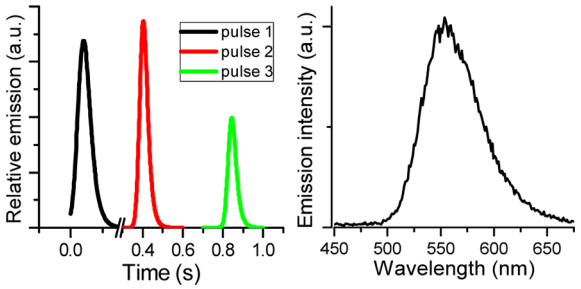

Figure 6. Global fitting of the time-resolved BL recorded in vivo from a firefly in the form of kinetic (left) and the spectral (right) components.

It is illustrative to compare the BL spectrum of the firefly recorded in vivo with the model data of OxyLH$_2$@Luc in solutions. Since the species of the firefly (collected in Georgia, USA) could not be identified, and the structure of its luciferase is unknown, direct analysis with the *L. cruciata* emission does not seem to be viable. Considering, however, that the emission spectra across the green-emitting firefly species are relatively consistent, the BL spectrum from Figure 6 can be qualitatively compared with the steady-state and time-resolved emission spectra from *L. cruciata*, shown in Figures 2c and 5 (Figure S5, Supporting Information).

The spectral width of the 550 nm BL band (fwhm 60 nm) of the firefly is much narrower than those of OxyLH$_2$@Luc steady-state emission at any pH, which could be an indication of fewer emitting species. On the other hand, the firefly BL and OxyLH$_2$@Luc SAS bands had comparable widths. It is tempting to assign the BL to one of the spectrally matched SAS, the closest one being the phenolate−enolate. However, our current data are insufficient to make such assignments because the luciferase structure is unknown. Nevertheless, this result could be important for further studies into the BL of living insects and other species.

CONCLUSIONS

In summary, we have demonstrated application of the global and target analysis to decipher the photoinduced dynamics of the firefly oxyluciferin/luciferase complex in buffer solutions, an extremely complex system that could not be analyzed by conventional approaches for spectral analysis. Due to the presence of multiple interconverting species in the ground state and excited state, six time-resolved decay surfaces were *simultaneously* fitted. The analysis afforded complete static and dynamic information on this multiluminophore in the active site of the luciferase. The results demonstrate the relevance of photoinduced proton transfer in the BL dynamics, and this could have implications on the proposed mechanisms for the color tuning of firefly BL. The model data were also compared to a time-resolved BL of living firefly. This experimental approach could be applied to further studies of similar complex BL systems in vitro and in vivo.

ASSOCIATED CONTENT

Supporting Information

The Supporting Information is available free of charge on the ACS Publications website at DOI: 10.1021/jacs.6b05078.

Time-resolved emission data of the studied systems; details of global and target analysis (PDF)

AUTHOR INFORMATION

Corresponding Authors

*pance.naumov@nyu.edu

*solntsev@gatech.edu

ORCID

Joris J. Snellenburg: 0000-0002-1428-0221

Panče Naumov: 0000-0003-2416-6569

Present Address

[#]Biological and Environmental Science & Engineering Division, King Abdullah University of Science and Technology, 4700 KAUST, Thuwal, 23955-6900 Saudi Arabia.

Author Contributions

[¶]J.J.S. and S.P.L. contributed equally to this work.

Notes

The authors declare the following competing financial interest(s): Richard DeSa and Kyril Solntsev are employed by OLIS, Inc.,which provided the RSM1000 spectrometer for this research.

ACKNOWLEDGMENTS

This work was supported by the U.S. National Science Foundation (CHE-1213047, K.M.S.), the Human Frontier Science Project grant (RGY0081/2011, P.N.), and New York University Abu Dhabi.

REFERENCES

(1) This article is part of the series "Photochemistry of "super" photoacids". The preliminary results presented in this article, including Figures 1 and 2, were reported in part at the 241st American Chemical Society National Meeting, 2011, Anaheim, CA (ORGN 665). For a preceding publication, see: Kuzmin, M. G.; Soboleva, I. V.; Ivanov, V. L.; Gould, E.-A.; Huppert, D.; Solntsev, K. M. *J. Phys. Chem. B* **2015**, *119*, 2444−2453.

(2) Ando, Y.; Niwa, K.; Yamada, N.; Enomoto, T.; Irie, T.; Kubota, H.; Ohmiya, Y.; Akiyama, H. *Nat. Photonics* **2008**, *2*, 44−47.

(3) Roura, S.; Gálvez-Montón, C.; Bayes-Genis, A. *J. Cell. Mol. Med.* **2013**, *17*, 693−703.

(4) Mezzanotte, L.; Que, I.; Kaijzel, E.; Branchini, B.; Roda, A.; Löwik, C. *PLoS One* **2011**, *6*, e19277.

DOI: 10.1021/jacs.6b05078
J. Am. Chem. Soc. 2016, 138, 16252−16258

(5) Shinde, R.; Perkins, J.; Contag, C. H. *Biochemistry* **2006**, *45*, 11103−11112.
(6) Greer, L. F.; Szalay, A. A. *Luminescence* **2002**, *17*, 43−74.
(7) Mezzanotte, L.; Que, I.; Kaijzel, E.; Branchini, B.; Roda, A.; Löwik, C. *PLoS One* **2011**, *6*, e19277−1−e19277−9.
(8) Foucault, M.-L.; Thomas, L.; Goussard, S.; Branchini, B. R.; Grillot-Courvalin, C. *Appl. Environ. Microbiol.* **2010**, *76*, 264−274.
(9) Minekawa, T.; Ohkuma, H.; Abe, K.; Maekawa, H.; Arakawa, H. *Luminescence* **2011**, *26*, 167−171.
(10) Takakura, H.; Kojima, R.; Urano, Y.; Terai, T.; Hanaoka, K.; Nagano, T. *Chem. - Asian J.* **2011**, *6*, 1800−1810.
(11) So, M.-K.; Xu, C.; Loening, A. M.; Gambhir, S. S.; Rao, J. *Nat. Biotechnol.* **2006**, *24*, 339−343.
(12) Naumov, P.; Ozawa, Y.; Ohkubo, K.; Fukuzumi, S. *J. Am. Chem. Soc.* **2009**, *131*, 11590−11605.
(13) Naumov, P.; Kochunnoonny, M. *J. Am. Chem. Soc.* **2010**, *132*, 11566−11579.
(14) Presiado, I.; Gepshtein, R.; Erez, Y.; Huppert, D. *J. Phys. Chem. A* **2011**, *115*, 7591−7601.
(15) Pinto da Silva, L.; Simkovitch, R.; Huppert, D.; Esteves da Silva, J. C. G. *ChemPhysChem* **2013**, *14*, 3441−3446.
(16) Solntsev, K. M.; Laptenok, S.; Naumov, P. *J. Am. Chem. Soc.* **2012**, *134*, 16452−16455.
(17) Støchkel, K.; Hansen, C. N.; Houmøller, J.; Nielsen, L. M.; Anggara, K.; Linares, M.; Norman, P.; Nogueira, F.; Maltsev, O. V.; Hintermann, L.; Nielsen, S. B.; Naumov, P.; Milne, B. F. *J. Am. Chem. Soc.* **2013**, *135*, 6485−6493.
(18) Rebarz, M.; Kukovec, B.-M.; Maltsev, O. V.; Ruckebusch, C.; Hintermann, L.; Naumov, P.; Sliwa, M. *Chem. Sci.* **2013**, *4*, 3803−3809.
(19) Wang, Y.; Hayamizu, Y.; Akiyama, H. *J. Phys. Chem. B* **2014**, *118*, 2070−2076.
(20) Ando, Y.; Akiyama, H. *Jpn. J. Appl. Phys.* **2010**, *49*, 117002−117008.
(21) Hiyama, M.; Akiyama, H.; Mochizuki, T.; Yamada, K.; Koga, N. *Photochem. Photobiol.* **2014**, *90*, 820−828.
(22) Maltsev, O. V.; Nath, N. K.; Naumov, P.; Hintermann, L. *Angew. Chem., Int. Ed.* **2014**, *53*, 847−850.
(23) Chen, S.-F.; Liu, Y.-J.; Navizet, I.; Ferré, N.; Fang, W.-H.; Lindh, R. *J. Chem. Theory Comput.* **2011**, *7*, 798−803.
(24) Liu, F.; Liu, Y.; De Vico, L.; Lindh, R. *J. Am. Chem. Soc.* **2009**, *131*, 6181−6188.
(25) Navizet, I.; Liu, Y.-J.; Ferré, N.; Roca-Sanjuán, D.; Lindh, R. *ChemPhysChem* **2011**, *12*, 3064−3076.
(26) Pinto da Silva, L.; Esteves da Silva, J. C. G. *J. Chem. Theory Comput.* **2011**, *7*, 809−817.
(27) Ren, A.-M.; Goddard, J. D. *J. Photochem. Photobiol., B* **2005**, *81*, 163−170.
(28) Orlova, G.; Goddard, J. D.; Brovko, L. Y. *J. Am. Chem. Soc.* **2003**, *125*, 6962−6971.
(29) Nakatani, N.; Hasegawa, J.; Nakatsuji, H. *J. Am. Chem. Soc.* **2007**, *129*, 8756−8765.
(30) Navizet, I.; Liu, Y.-J.; Ferré, N.; Xiao, H.-Y.; Fang, W.-H; Lindh, R. *J. Am. Chem. Soc.* **2010**, *132*, 706−712.
(31) Song, C.-I.; Rhee, Y. M. *J. Am. Chem. Soc.* **2011**, *133*, 12040−12049.
(32) Shimomura, O. *Bioluminescence: Chemical Principles and Applications*; World Scientific: Singapore, 2008; pp 151−153.
(33) Pinto da Silva, L.; Esteves da Silva, J. C. G. *ChemPhysChem* **2015**, *16*, 455−464.
(34) Hirano, T.; Hasumi, Y.; Ohtsuka, K.; Maki, S.; Niwa, H.; Yamaji, M.; Hashizume, D. *J. Am. Chem. Soc.* **2009**, *131*, 2385−2396.
(35) Maltsev, O. V.; Yue, L.; Rebarz, M.; Hintermann, L.; Sliwa, M.; Ruckebusch, C.; Pejov, L.; Liu, Y.; Naumov, P. *Chem. - Eur. J.* **2014**, *20*, 10782−10790.
(36) Ghose, A.; Rebarz, M.; Maltsev, O. V.; Hintermann, L.; Ruckebusch, C.; Fron, E.; Hofkens, J.; Mély, Y.; Naumov, P.; Sliwa, M.; Didier, P. *J. Phys. Chem. B* **2015**, *119*, 2638−2649.
(37) Nakatsu, T.; Ichiyama, S.; Hiratake, J.; Saldanha, A.; Kobashi, N.; Sakata, K.; Kato, K. *Nature* **2006**, *440*, 372−376.
(38) White, E. H.; Roswell, D. F. *Photochem. Photobiol.* **1991**, *53*, 131−136.
(39) Gandelman, O. A.; Brovko, L. Y.; Ugarova, N. N.; Chikishev, A. Y.; Shkurimov, A. P. *J. Photochem. Photobiol., B* **1993**, *19*, 187−191.
(40) We propose three reasons for the slightly increased fluorescence lifetime in the case of e3 excited at 467 nm: (a) The IRF is about 120 ps longer than that currently modeled (the assumption is that the IRFs of e1, e2, and e3 data sets are identical). (b) The data show photoexcited conversion of phenolate−enolate to phenolate−enol, as well as the reverse reaction. (c) The data are indicative of relatively slow conversion of phenolate−enol to phenolate−enolate.
(41) van Stokkum, I. H. M.; Larsen, D. S.; van Grondelle, R. *Biochim. Biophys. Acta, Bioenerg.* **2004**, *1657*, 82−104.
(42) Welsh, D. K.; Kay, S. A. *Curr. Opin. Biotechnol.* **2005**, *16*, 73−78.
(43) Zhao, H.; Doyle, T. C.; Coquoz, O.; Kalish, F.; Rice, B. W.; Contag, C. H. *J. Biomed. Opt.* **2005**, *10*, 041210.
(44) Lall, A. B.; Cronin, T. W.; Carvalho, A. A.; de Souza, J. M.; Barros, M. P.; Stevani, C. V.; Bechara, E. J.; Ventura, D. F.; Viviani, V. R.; Hill, A. A. *J. Comp. Physiol., A* **2010**, *196*, 629−638.
(45) Oba, Y.; Furuhashi, M.; Bessho, M.; Sagawa, S.; Ikeya, H.; Inouye, S. *Photochem. Photobiol. Sci.* **2013**, *12*, 854−863.
(46) Snellenburg, J. J.; Laptenok, S. P.; Seger, R.; Mullen, K. M.; van Stokkum, I. H. M. *J. Stat. Soft.* **2012**, *49*, 1−23.
(47) Publicly available at http://www.glotaran.org.

DOI: 10.1021/jacs.6b05078
J. Am. Chem. Soc. 2016, 138, 16252−16258